

## Behavior of the multiplicity with large perpendicular momentum transferred to the leading proton as predicted by multiple quark scattering\*

A. S. Kanofsky

*Department of Physics, Lehigh University, Bethlehem, Pennsylvania 18015  
and Brookhaven National Laboratory, Upton, New York 11973*

(Received 3 June 1974; revised manuscript received 16 July 1975)

The previous calculation used to explain the rise in multiplicity with increasing  $p_{\perp}$  given to the leading proton has been extended to include higher order quark-quark scattering terms. It is found that another abrupt rise in the multiplicity can be expected at  $p_{\perp} \sim 1.5$  GeV/c where third-order inelastic scattering terms begin to dominate over second-order terms.

In a recent experiment, Ramanaukas *et al.*<sup>1</sup> have determined that the multiplicity increases with increasing perpendicular momentum,  $p_{\perp}$ , transferred to the leading proton. In a recent paper,<sup>2</sup> Klenk and I explained this effect as being due to second-order inelastic scattering terms dominating over first-order scattering terms at higher values of  $p_{\perp}$ . The abrupt rise in the multiplicity, starting at  $p_{\perp} \sim 0.65$  GeV/c could be simply explained as due to the onset of the dominance of quark double inelastic scattering over single quark inelastic scattering, where for  $p_{\perp} < 0.65$  GeV/c only single quark inelastic scattering existed.

The rise was followed by a plateau which was due only to the double inelastic terms dominating. No higher-order diagrams were included in the calculation. Also, no attempt was made to vary the quark inelastic scattering parameters from the elastic case, the results being consistent with the data as it existed at the time.

Presented here are the results of including higher-order terms and allowing the inelastic scattering amplitude parameters to vary, and we make predictions on the behavior of multiplicity with even higher  $p_{\perp}$ . Also, predictions are made for Fermilab energies ( $s = 200$  GeV<sup>2</sup> and 400 GeV<sup>2</sup>). As before, the quark-quark inelastic scattering amplitude is parameterized as

$$f(\Delta) = f'_0 e^{-b'^2 \Delta^2}, \quad (1)$$

where  $f'_0 = f'_R + if'_I$ ,  $b'^2 = b'^2_R + ib'^2_I$ , and  $\Delta$  is the momentum transferred between the quarks. Here  $f'_R$  and  $f'_I$  are the real and imaginary parts respectively, of the inelastic quark-quark forward scattering amplitude and  $b'^2_R$  and  $b'^2_I$  are the real and imaginary exponent coefficients.

The quark-quark elastic amplitude has the same functional form, but with independent unprimed parameters. The elastic parameters are taken the same as previously determined from elastic

$p$ - $p$  scattering.<sup>3</sup>

$$b_R^2 = 0.01, \quad b_I^2 = -47.4 + 13.1 \ln s,$$

$$A(s) = 4.54 + 1.0 \ln s, \quad f_R = 0.05, \quad f_I = 1.1, \quad (2)$$

where  $s$  is the c.m. energy squared and all units are in (GeV/c)<sup>-2</sup>. The proton wave-function absolute value squared is

$$|\Psi(\vec{r}_1, \vec{r}_2, \vec{r}_3)|^2 = e^{-w^2(\vec{r}_1 + \vec{r}_2 + \vec{r}_3)^2} \delta(\vec{r}_1 + \vec{r}_2 + \vec{r}_3).$$

Here  $w^2 = 8/(3a_p^2)$  and  $a_p^2 = [A(s) - b_R^2]/2.0$ .

Figure 1 illustrates the inelastic scattering

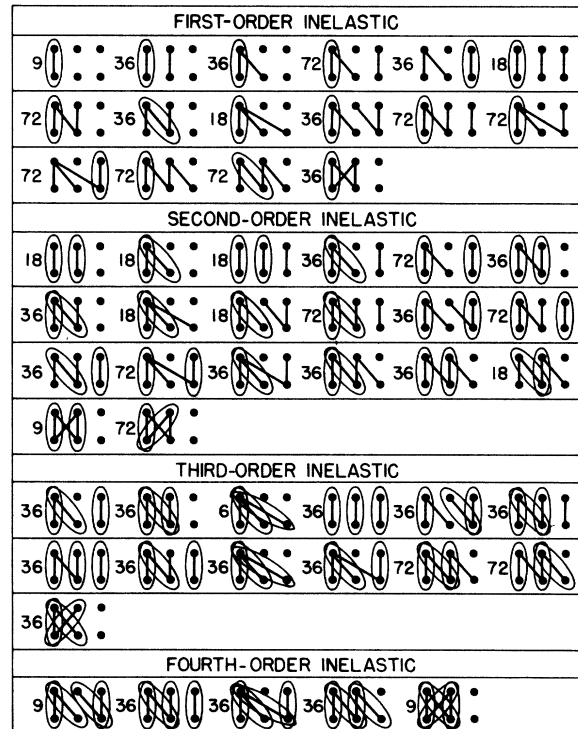


FIG. 1. Inelastic scattering diagrams up to and including fourth-order inelastic ones. The ellipses represent inelastic quark-quark scattering processes, the lines elastic processes.

diagrams for higher orders. Ellipses (with lines) represent inelastic scattering and lines alone represent elastic scattering. The number of distinct diagrams is given next to each diagram. A dot represents a quark — the upper and lower dots being the three quarks in each proton.

These diagrams can be evaluated analytically.<sup>4</sup> Each diagram can be represented as an inte-

gration of exponential terms in  $\vec{r}_1, \vec{r}_2, \vec{r}_3$  and  $\vec{r}'_1, \vec{r}'_2, \vec{r}'_3$  and the impact parameter,  $b$ , which is the projection along the plane normal to the incoming momentum of the vector connecting the proton centers. For example, the amplitude for the third-order inelastic diagram of Fig. 1 can be evaluated by the integral

$$F(\Delta) = \int e^{i\vec{\Delta} \cdot \vec{b}} d^2b \int d^3r_1 d^3r_2 d^3r_3 d^3r'_1 d^3r'_2 d^3r'_3 e^{-w^2(\vec{r}_1 + \vec{r}_2 + \vec{r}_3)^2} \delta(\vec{r}_1 + \vec{r}_2 + \vec{r}_3) \times e^{-w^2(\vec{r}'_1 + \vec{r}'_2 + \vec{r}'_3)^2} \delta(\vec{r}'_1 + \vec{r}'_2 + \vec{r}'_3) \Gamma(b + \vec{r}_1 - \vec{r}'_1) \Gamma(b + \vec{r}_1 - \vec{r}'_2) \Gamma(b + \vec{r}_3 - \vec{r}'_3), \quad (3)$$

where the  $\Gamma$ 's are related to the scattering amplitudes by

$$\Gamma(r) = \int d^2\Delta f(\Delta) e^{i\vec{\Delta} \cdot \vec{r}}.$$

The total inelastic cross section,  $F(\Delta, m)$ , for production of  $m$  pions at momentum transfer  $\Delta$  can then be calculated: ( $\Delta = p_\perp$ )

$$F(\Delta, m) = F_1(\Delta) P(1; m) + F_2(\Delta) P(2; m) + F_3(\Delta) P(3; m) + F_4(\Delta) P(4; m) \quad (4)$$

where

$$F_1(\Delta) = \sum_i |F_1^i|^2, \quad F_2(\Delta) = \sum_i |F_2^i|^2, \quad F_3(\Delta) = \sum_i |F_3^i|^2, \dots, \quad (5)$$

and  $F_i^i$  is the amplitude for the  $i$ th diagram of the  $l$ th-order inelastic scattering (as shown in Fig. 1), evaluated at momentum transfer  $\Delta$ . The  $P$ 's are generated from a Poisson distribution according to the following formulas:

$$P(1; m) = \frac{\mu^m e^{-\mu}}{m!}, \quad P(2; m) = \sum_k \frac{\mu^{m-k} e^{-\mu}}{(m-k)!} \frac{\mu^k e^{-\mu}}{k!}, \quad P(3; m) = \sum_k P(2; k) P(1; m-k), \quad (6) \quad P(4; m) = \sum_k P(3; k) P(1; m-k).$$

Here  $\mu$  is the average number of pions produced in a collision, and  $P(k; m)$  is the probability that a  $k$ th-order scatter will produce  $m$  particles.

Thus, to summarize, the total inelastic scat-

tering amplitude is given by taking each diagram, multiplying by the number of distinct ways the diagram can occur, taking the absolute value squared of this quantity, and then summing over all diagrams. The sum of  $k$ th-order diagrams then multiplies the Poisson-generated probabilities for getting  $m$  particles from a  $k$ th-order collision. This is shown schematically in Fig. 2.

It is then possible to calculate the average multiplicity,  $\bar{m}$ , from the  $F(\Delta, m)$ 's:

$$\bar{m} = \sum_m F(\Delta, m) m / \sum_m F(\Delta, m). \quad (7)$$

The results are shown in Fig. 3 for various values of the average number,  $\mu$ , of pions produced per collision for  $s = 60$  (GeV)<sup>2</sup>, the value for the data of Ramanaukas *et al.* The elastic and inelastic scattering parameters are taken the same with  $A(s) = 8.63$  and  $b_r^2 = 6.24$ . It is seen from the figure that the multiplicity should be expected to undergo a second rise at a value of  $p_\perp \sim 1.5$  GeV/ $c$ , where triple scattering begins to dominate over second-order scattering.

Figure 4 illustrates how the multiplicity varies with the inelastic scattering parameters. A distinct plateau in the third and fourth-order scattering region is not indicated for any value of the scattering parameters. But for all cases, the first plateau exists to a greater or lesser extent as well as the rise at  $p_\perp \sim 1.5$  GeV/ $c$ . In the first plateau region the multiplicity is not constant but increases at a rate dependent on parameters. A rise in multiplicity in this region is seen already in the more recent high-statistics, high- $p_\perp$ , data of Schübelin *et al.*<sup>5</sup> It is not necessary to include the third and higher-order inelastic scattering terms to get this increase. The calculated multiplicity with only second-order terms included is also shown in Fig. 3 (dash-dot-dash

$$\begin{aligned}
 F(\Delta, m) = & \left[ 9X \left( \text{diagram} \right)^2 + 36X \left( \text{diagram} \right)^2 + 72X \left( \text{diagram} \right)^2 \right. \\
 & + \left. 36X \left( \text{diagram} \right)^2 + 18X \left( \text{diagram} \right)^2 + 72X \left( \text{diagram} \right)^2 \right. \\
 & + \left. 36X \left( \text{diagram} \right)^2 + 18X \left( \text{diagram} \right)^2 + 36X \left( \text{diagram} \right)^2 \right. \\
 & + \left. 72X \left( \text{diagram} \right)^2 + 72X \left( \text{diagram} \right)^2 + \dots \right] \frac{\mu^m e^{-\mu}}{m!} \\
 & + \left[ 18X \left( \text{diagram} \right)^2 + 18X \left( \text{diagram} \right)^2 + 18X \left( \text{diagram} \right)^2 \right. \\
 & + \left. 36X \left( \text{diagram} \right)^2 + 72X \left( \text{diagram} \right)^2 + 36X \left( \text{diagram} \right)^2 \right. \\
 & + \left. 36X \left( \text{diagram} \right)^2 + 18X \left( \text{diagram} \right)^2 + 18X \left( \text{diagram} \right)^2 \right. \\
 & + \left. 72X \left( \text{diagram} \right)^2 + \dots \right] \sum_k \left( \frac{\mu^{m-k} e^{-\mu}}{(m-k)!} \right) \left( \frac{\mu^k e^{-\mu}}{k!} \right) \\
 & + \left[ 36X \left( \text{diagram} \right)^2 + 36X \left( \text{diagram} \right)^2 + 6X \left( \text{diagram} \right)^2 \right. \\
 & + \left. 36X \left( \text{diagram} \right)^2 + 36X \left( \text{diagram} \right)^2 + 36X \left( \text{diagram} \right)^2 \right. \\
 & + \left. 36X \left( \text{diagram} \right)^2 + \dots \right] \sum_{m'} \left[ \sum_k \left( \frac{\mu^{m'-k} e^{-\mu}}{(m'-k)!} \right) \left( \frac{\mu^k e^{-\mu}}{k!} \right) \right] \frac{\mu^{m-m'} e^{-\mu}}{(m-m')!} \\
 & + \left[ 9X \left( \text{diagram} \right)^2 + 36X \left( \text{diagram} \right)^2 + 36X \left( \text{diagram} \right)^2 \right. \\
 & + \left. 36X \left( \text{diagram} \right)^2 + 9X \left( \text{diagram} \right)^2 \right] \sum_k P(3; k) \frac{\mu^{m-k} e^{-\mu}}{(m-k)!}
 \end{aligned}$$

FIG. 2. Schematic representation of this calculation. See the text for details.

line), and the multiplicity for this case increases gradually until a  $p_{\perp}$  value of 1.5, where the third- and fourth-order diagrams for second-order inelastic scattering become large. Also, from Fig. 4, it is seen that in order to obtain the most distinct plateau, the inelastic and elastic scattering parameters should be equal, in agreement with our previous statements.<sup>3</sup>

It is possible also to plot up the actual multiplicity distributions in both the single scattering region, double scattering region (first plateau), and triple scattering region. These are shown in Fig. 5 for the various regions and for various values of  $\mu$ , the multiplicity parameter. For the first- and second-order scattering regions, the distributions look very much like Poisson distributions with a shift of the mean and some broadening in the second-order region.

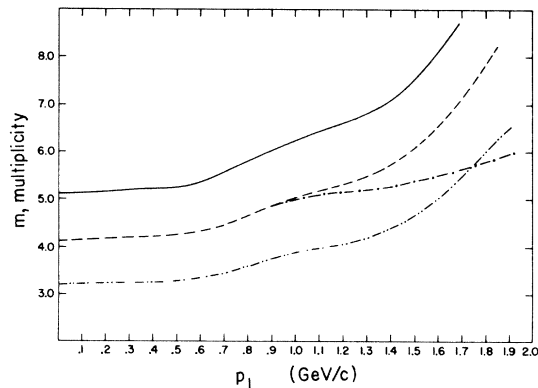


FIG. 3. Multiplicity distributions for various values of  $\mu$ , where  $\mu$  is the average number of  $\pi$ 's produced per collision. Also, with third- and fourth-order inelastic terms not included.  $\mu = 3$ , dash-dot-dot-dash line;  $\mu = 4$  dashed line;  $\mu = 5$ , solid line.

Taking the elastic and inelastic parameters the same, and knowing how the elastic parameters vary with c.m. energy, it is possible to make predictions for the behavior of the multiplicity increase at Fermilab energies. Shown in Fig. 6 are plots of the multiplicity as a function of  $p_{\perp}$  for  $s = 400 \text{ GeV}^2$  and  $s = 200 \text{ GeV}^2$ . The plateau is even more pronounced than at lower energies. Future experiments will hopefully confirm the high- $p_{\perp}$  predictions.

In effect, what we have calculated is the differential cross section  $d\sigma/dt$  as a function of the  $p_{\perp}$  given to "the excited system" of pions and original proton. This is, of course, not the  $p_{\perp}$  distribution given to the proton which is finally observed in the ARGO Brookhaven particle spectrometer experiments of Turkot *et al.*

To determine what the  $p_{\perp}$  distribution of the proton is, we must determine the correlation of the  $p_{\perp}$  of the excited system with the  $p_{\perp}$  of the proton. To do this, we have generated Monte Carlo events in a two-fireball model. Here, one or both protons are considered to become fireballs which emit pions and a single proton. The distribution in  $p_{\perp, p}$  of the proton is then calculated as a function of the  $p_{\perp, f}$  of the fireball and the invariant mass, MM, of the particles other than the proton. We show in Fig. 7 such a distribution in  $p_{\perp, p}$  for fixed MM and  $p_{\perp, f}$  (600 MeV/c) near the Glauber-model breakpoint, 0.65 GeV/c, and for fixed fireball masses.

Now, the differential cross section for the fireballs,  $d\sigma/dt_f$  is a sharply dropping function (orders of magnitude) of  $p_{\perp, f}$ , and the effect this has on the  $p_{\perp, p}$  distribution is that the main contribution to the proton differential cross section  $d\sigma/dt_p$  comes from the lowest possible momentum for the fireball which can still result in the observed  $p_{\perp, p}$  value. This is shown schematically in Fig. 8. This has the effect of shifting the breakpoint for multiplicity to higher momentum transfer.

Also, we notice for fixed masses of the fireballs that as the MM value increases, the maximum  $p_{\perp, p}$  value for the proton decreases, which corresponds to a shift in  $p_{\perp, p}$  to smaller values (for fixed  $p_{\perp, f}$ ) as the MM increases. This is also seen in the data of Turkot *et al.*

Similar results can be obtained for the pion distributions and explain why the multiplicity increases with increasing perpendicular momentum to the pion.<sup>7</sup> To give an idea of the magnitude of the momentum shifts, we plot in Fig. 9 the maximum  $p_{\perp, p}$  values for which the  $p_{\perp, p}$  distribution drops to zero— $p_{\perp, p}^0$  versus  $p_{\perp, f}$  for various MM and fireball values for the  $p2\pi$  fireball decays.

Also, we plot in Fig. 10 the value of  $p_{\perp, p}^0$  as a

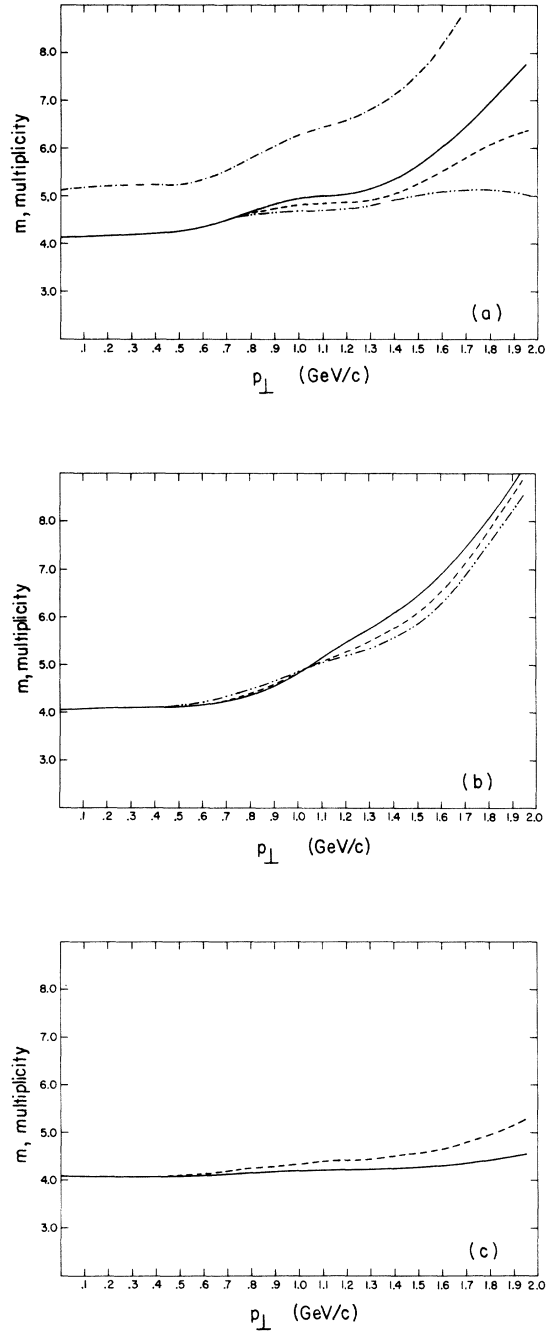


FIG. 4. Multiplicity versus  $p_{\perp}$  for various values of the inelastic scattering parameters. Elastic parameters:  $b_R'^2 = 0.01$ ,  $b_I'^2(60) = 6.24$ ,  $A(60) = 8.63$ ,  $f_R = 0.05$ ,  $f_I = 1.1$ . (a) Variation of  $b_R'^2$ , all other inelastic parameters same as elastic.  $\mu = 5$ ,  $b_R'^2 = 0.01$ , dash-dot-dash line.  $\mu = 4$ ,  $b_R'^2 = 1.0$ , solid line.  $\mu = 4$ ,  $b_R'^2 = 2.0$ , dash-dash line;  $b_R'^2 = 4.0$ , dash-dot-dot line. (b) Variation of  $b_I'^2$ ; all other inelastic parameters same as elastic  $\mu = 4$ ,  $b_I'^2 = -10.26$  solid line;  $b_I'^2 = -0.26$  dash-dot-dot line;  $b_I'^2 = -5.26$  dash-dot line. (c) Variation of  $f_I$ ; all other inelastic parameters same as elastic.  $\mu = 4$ ,  $f_I' = 0.5$ , dash-dash line.  $\mu = 4$ ,  $f_I' = 0.3$ , solid line.

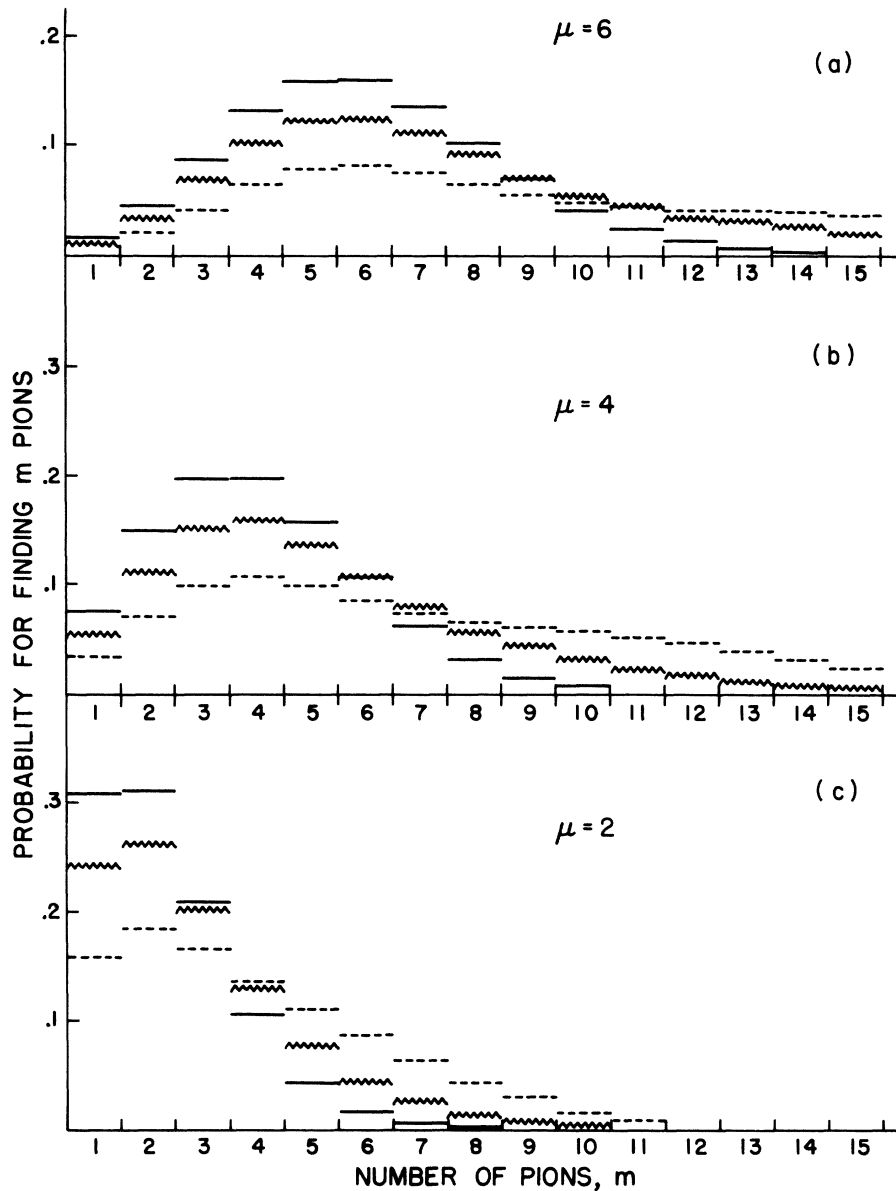


FIG. 5. Particle-number distributions for the various scattering regions. (a)  $\mu = 6$ ,  $p_{\perp} = 0.0$  GeV/c, solid line;  $p_{\perp} = 1.2$  GeV/c, wavy line;  $p_{\perp} = 1.7$  GeV/c, dashed line. (b)  $\mu = 4$ ,  $p_{\perp} = 0.0$  GeV/c, solid line;  $p_{\perp} = 1.2$  GeV/c, wavy line;  $p_{\perp} = 1.7$  GeV/c, dashed line. (c)  $\mu = 2$ ,  $p_{\perp} = 0.0$  GeV/c, solid line;  $p_{\perp} = 1.2$  GeV/c, wavy line;  $p_{\perp} = 1.7$  GeV/c, dashed line.

function of the parent fireball mass and indicate how it depends on the other fireball mass. If we are to obtain agreement with the Turkot data, we require the correct shift of  $p_{\perp, p}^0$  away from the break-point value for  $p_{\perp, f}$  as calculated from our model. We can locate the break-point  $p_{\perp, p}^0$  value correctly by choosing the correct masses for the fireballs, since  $p_{\perp, p}^0$  is a function of the fireball

masses. Looking at Fig. 10 and comparing the break-point values for the experimental data ( $\sim 0.8$  GeV/c) and the theoretical Glauber model (0.65 GeV/c) for the 5200-MeV missing-mass curve, we get fireball masses of  $\sim 1800$  MeV as being reasonable. Now, for the case of the  $p4\pi$  decay, as shown in Fig. 11, the  $p_{\perp, p}^0$  points are all shifted toward lower momentum values. There

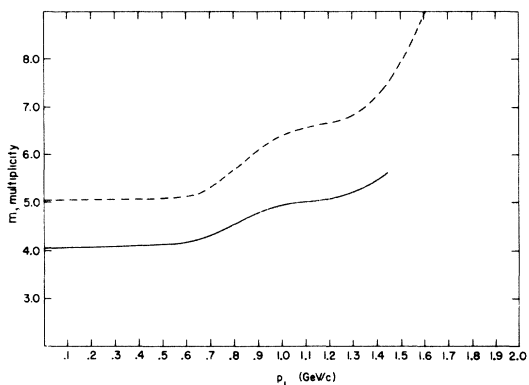


FIG. 6. Multiplicity versus  $p_{\perp}$  for Fermilab energies. Parameter values given by equations in text.  $s = 200 \text{ GeV}^2$ , solid lines.  $s = 400 \text{ GeV}^2$ , dashed lines.

would certainly be more  $p4\pi$  than  $p2\pi$  breakup at the higher MM since the charged multiplicity in the Turkot *et al.* data increases up to an average of 6 with increasing MM. To get agreement here the fireball masses are  $\sim 2200 \text{ MeV}$ . Thus, we would expect higher fireball masses for  $p4\pi$  decays.

In conclusion, the inclusion of higher-order quark scattering diagrams predicts additional structure and an increase in the multiplicity with increasing  $p_{\perp}$ . Also, we see that it is possible to obtain the correct shifts of the break point with MM and the observed proton perpendicular momentum values seen in the Turkot data if the Glauber model of Kanofsky and Klenk is folded into a Monte Carlo decay model.

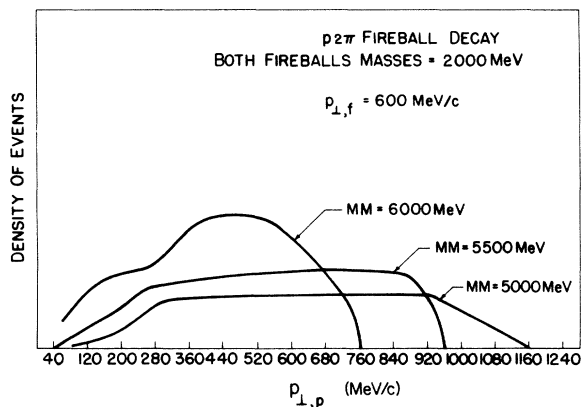


FIG. 7. Distribution in events as a function of the proton perpendicular momentum,  $p_{\perp,p}$ , for fixed fireball perpendicular momentum,  $p_{\perp,f}$ , of  $600 \text{ MeV}/c$ , fixed fireball masses and several fixed missing masses MM off of the proton.

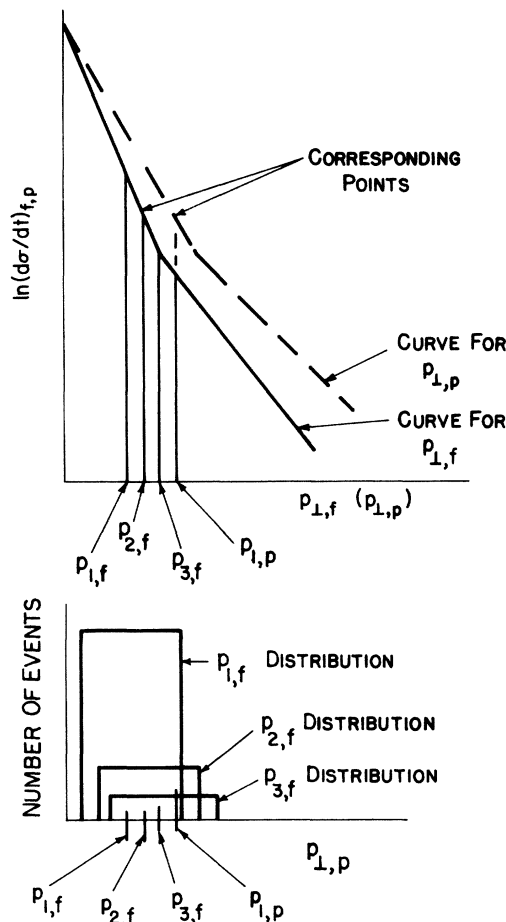


FIG. 8. Schematic illustration of regions of  $d\sigma/dt_f$  curve for fireball which contribute to  $d\sigma/dt_p$  for observed proton. The quantities  $p_{1,f}$ ,  $p_{2,f}$ ,  $p_{3,f}$  are the fireball perpendicular momentum which contribute to an observed proton perpendicular momentum of  $p_{1,p}$ .

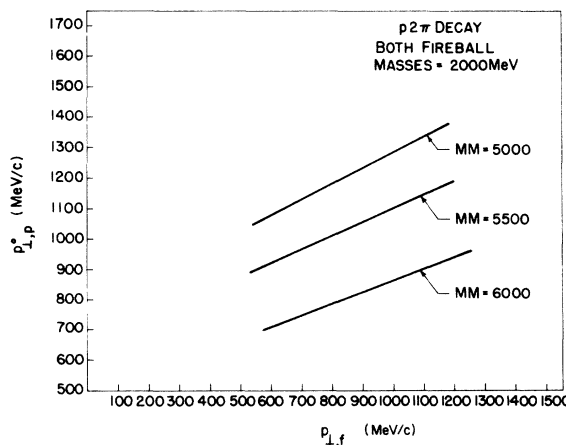


FIG. 9. Values of  $p_{\perp,p}$  for which the distribution drops to zero,  $p_{\perp,p}^0$ , as a function of  $p_{\perp,f}$  for various MM and fireball masses of  $p2\pi$  decays.

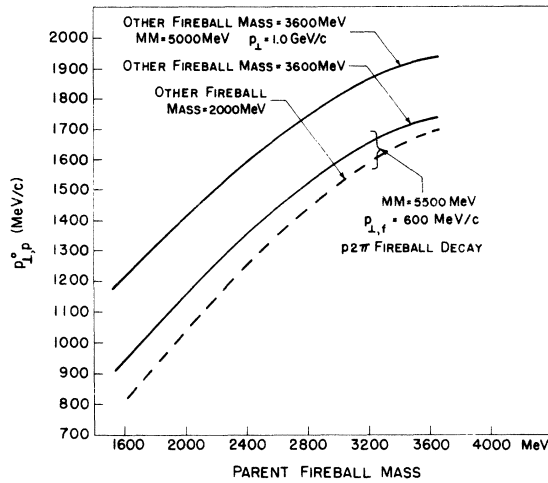


FIG. 10. Value of  $p_{\perp,p}^0$  as a function of parent fireball mass with fixed  $p_{\perp,f}$  for the case of  $p2\pi$  decays.

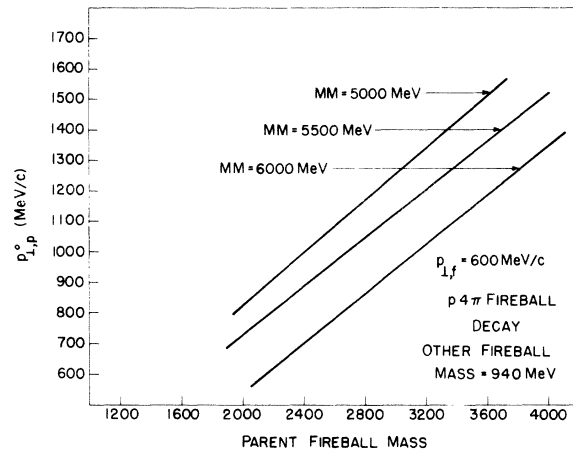


FIG. 11. Value of  $p_{\perp,p}^0$  as a function of parent fireball mass with fixed  $p_{\perp,f}$  for the case of  $p4\pi$  decays.

#### ACKNOWLEDGMENTS

The author would like to thank Dr. Frank Turkot and members of the ARGO group for their support

and encouragement. He also thanks D. Allen and G. Gerhab for their assistance with the Monte Carlo fireball program.

\*Work supported in part by the U. S. Energy Research and Development Administration.

<sup>1</sup>A. Ramanaukas *et al.*, Phys. Rev. Lett. **31**, 1371 (1973).

<sup>2</sup>A. S. Kanofsky and K. F. Klenk, Phys. Rev. Lett. **31**, 1323 (1973).

<sup>3</sup>K. F. Klenk and A. S. Kanofsky, Phys. Lett. **44B**, 383 (1973).

<sup>4</sup>K. F. Klenk and A. S. Kanofsky, Nuovo Cimento **13A**, 446 (1973); K. F. Klenk, Ph. D. thesis, Lehigh University, 1973 (unpublished).

<sup>5</sup>P. Schübelin *et al.*, Bull. Am. Phys. Soc. **19**, 466 (1974).

<sup>6</sup>A. S. Kanofsky *et al.* (unpublished).

<sup>7</sup>E. W. Anderson *et al.*, Phys. Rev. Lett. **34**, 294 (1975).